





Measurement and analysis of the isomeric cross section ratios for the ^{94}Tc nucleus

G. S. Li ^{1,2}, Y. D. Fang,^{1,*} X. H. Zhou,^{1,†} A. Diaz-Torres ³, A. Rohilla ¹, M. L. Liu,¹ N. T. Zhang,¹ Y. H. Zhang,¹ J. G. Wang,¹ B. S. Gao,¹ Y. H. Qiang,¹ S. Guo,¹ S. C. Wang,¹ Y. Zheng,¹ J. Lubian ⁴ and H. O. Soler ⁴

¹CAS Key Laboratory of High Precision Nuclear Spectroscopy, Institute of Modern Physics, Chinese Academy of Sciences, Lanzhou 73000, People's Republic of China

²School of Nuclear Science and Technology, University of Chinese Academy of Sciences, Beijing 100049, People's Republic of China

³Department of Physics, University of Surrey, Guildford GU2 7XH, United Kingdom

⁴Instituto de Física, Universidade Federal Fluminense, Avenida Litorânea s/n, Gragoatá, Niterói, Rio de Janeiro 24210-340, Brazil



(Received 19 July 2020; revised 21 September 2020; accepted 20 October 2020; published 12 November 2020)

We report on an isomer yield ratio study of biologically important ^{94}Tc following the fusion of the $^9\text{Be} + ^{89}\text{Y}$ system, carried out using the offline γ -ray spectroscopy in continuation to the online activation method. The incident beam energies considered are above the Coulomb barrier for the present paper. The PLATYPUS model in conjunction with a potential model calculation was employed to analyze the data. An agreement in the order of magnitude between the experimental data and the theoretical predictions has been achieved by applying a phenomenological approach. The approach was further tested with isomer yield ratios of ^{94}Tc formed through $^3\text{He} + ^{93}\text{Nb}$ reactions. Possible factors that relate to the isomer yield ratios are also presented.

DOI: [10.1103/PhysRevC.102.054607](https://doi.org/10.1103/PhysRevC.102.054607)

I. INTRODUCTION

In recent years, the investigation into technetium (Tc) isotopes has been a subject of intense experimental and theoretical studies due to its practical applications, especially in the nuclear medicine field. For example, the γ ray emitted by $^{99}\text{Tc}^m$ is widely used for medical diagnostic studies. Different chemical forms have been used for brain, bone, liver, spleen, and kidney imaging as well as blood flow studies [1]. This is benefited from the fact that the $^{99}\text{Tc}^m$ has a short half-life ($T_{1/2} = 6.01$ h) and does not remain in the body for a long time. The neutron-deficient Tc isotopes, on the other hand, are also suggested as suitable candidates for medical diagnosis. For instance, the calculated γ -ray intensities of $^{95}\text{Tc}^g$ and $^{96}\text{Tc}^g$ nuclei injected into the human body are 63% and 70% respectively, relative to that of a $^{99}\text{Tc}^m$ nucleus, suggesting that the two nuclei can also work as γ -ray emitters of diagnosis [2]. Other than these nuclei, the $^{94}\text{Tc}^m$ with large positron branching ratio (70%) and medium positron end-point energy (2.4 MeV) is a suitable candidate for positron emission tomography and regarded as an intriguing alternative to many already popular tracers [3–5].

Various nuclear reactions have been employed in the production for Tc isotopes, such as (p, n) , (n, p) , and deuterium-induced reactions [6–9]. In addition, large numbers of studies on the excitation functions related to the isotopes are also available from the literature [10–13]. However, most of these studies are based on the light-ion-induced reactions, and cross-section data with heavy-ion-induced reactions are scarce. Maiti and Lahiri [14] have reported on new routes of

Tc isotope production using the $^7\text{Li} + ^{\text{nat}}\text{Zr}$ and $^9\text{Be} + ^{\text{nat}}\text{Y}$ reactions, and the excitation functions were given. Some functions are also available from the $^{12}\text{C} + ^{89}\text{Y}$ and $^9\text{Be} + ^{89}\text{Y}$ reactions [15,16], focusing on the complete fusion (CF) and incomplete fusion studies. Still, the data on the heavy-ion-induced reactions and related reaction mechanisms for the production of Tc isotopes are in high demand.

To shed light on the nuclear data of proton-rich Tc isotopes, we have investigated the production of ^{94}Tc formed through the $^9\text{Be} + ^{89}\text{Y}$ reactions, focusing on the population of different states. Since the ^9Be projectile is weakly bound with unusual nucleon distributions, the special (such as large probability of breakup before the reaction) can give strong influence to the interaction process. This makes the status of residues (e.g., from the CF following breakup) different compared to the fusion reaction cases induced by stable bound projectiles, such as α , ^{12}C , etc. In this context, the study will open the opportunity to compare other projectile-target combinations to further explore the underlying reaction dynamics. Specifically, the ^{94}Tc has an isomeric state of $(2)^+$ and ground state of 7^+ with different characteristic γ rays from their decays. This will allow the determination of isomer yield ratios to get access to the information on the production mechanism, in particular, on the angular momentum of excited states of the precursor. We note that the experimental data related to the isomer yield ratio are still scarce in the literature. From the theoretical point of view, different types of models are available to describe the reaction mechanisms, ranging from classical to quantum-mechanical methods [17–21]. Among them, the PLATYPUS model [22] could offer special opportunity to the weakly bound projectile studies as it uses classical trajectories in conjunction with stochastic breakup. It is meaningful to test the models with available experimental data.

*fangyd@impcas.ac.cn

†zxh@impcas.ac.cn

This paper presents the experimental isomer yield ratios in ^{94}Tc , a study of the data by employing the PLATYPUS model combined with potential model calculation. The experimental setup and procedure are described in Sec. II. In Sec. III we present the measured spectra, data analysis, as well as the results. Comparisons of the data with theoretical calculations are shown in Sec. IV. The conclusions drawn from the present paper are given in Sec. V.

II. EXPERIMENTAL DETAILS

The measurement was performed by the stacked-foil activation technique followed by offline identification of the characteristic γ rays of the reaction residues. The detailed descriptions of the setup and the experimental technique can be found in Ref. [23], and only a brief description is given in the present context. The collimated ^9Be beam was delivered by the Heavy Ion Research Facility in Lanzhou. Five ^{89}Y targets having thickness ≈ 1.0 mg/cm 2 were irradiated for about 12 h at an average beam current of 13 nA. The targets were backed with Au for reducing the energy of the beam on the subsequent target. The initial energy, delivered by the accelerator, was 50.4 MeV. The effective incident energy on each ^{89}Y target was taken as that bombarded at half the target thickness. It was obtained by ATIMA calculation, incorporated within the LISE++ program [24,25]. Finally, the irradiation of the targets was performed in the energy range of 45.9–50.1 MeV in steps of 1–1.1 MeV. The beam flux was extracted using a precise current-integrator device from the charge collected at the Faraday cup, which is biased with a -400 -V electrode and installed at the back of targets, following the direction of beam flow. The precise current-integrator device can ensure us to extract the beam intensity at regular intervals of 1 s. Additionally, to cross-check the beam flux that impinged on the targets, two silicon detectors were mounted at $\pm 30^\circ$ with respect to the beam line. The elastic scattered ^9Be projectiles by a thin Au foil, installed upstream from the targets were monitored. The two sets of deduced beam currents were found to be in agreement with each other.

After the online beam irradiation, the activated targets were transferred to a separate laboratory for performing offline measurements. A setup formed by five high-purity germanium (HPGe) detector groups was used. Each group composed of two HPGe detectors placed at an angle of 180° to each other. This allows the acquisition of data possible both in singles as well as in γ - γ coincidence mode at the same instance by placing the activated targets at the optimized distances. Further to reduce the γ rays due to natural background, the Ge crystal of each detector was shielded with an annular cylinder of Pb material having thickness of 3 cm, making the acquitted spectra more fine. The γ sources of ^{60}Co , ^{133}Ba , and ^{152}Eu were used to calculate the absolute efficiency of the detectors. The radioactive sources and the targets were counted in the same geometry.

III. DATA ANALYSIS AND RESULTS

The residues of the $^9\text{Be} + ^{89}\text{Y}$ reaction system covered in the present measurement are mainly from the $3n$, $4n$, and

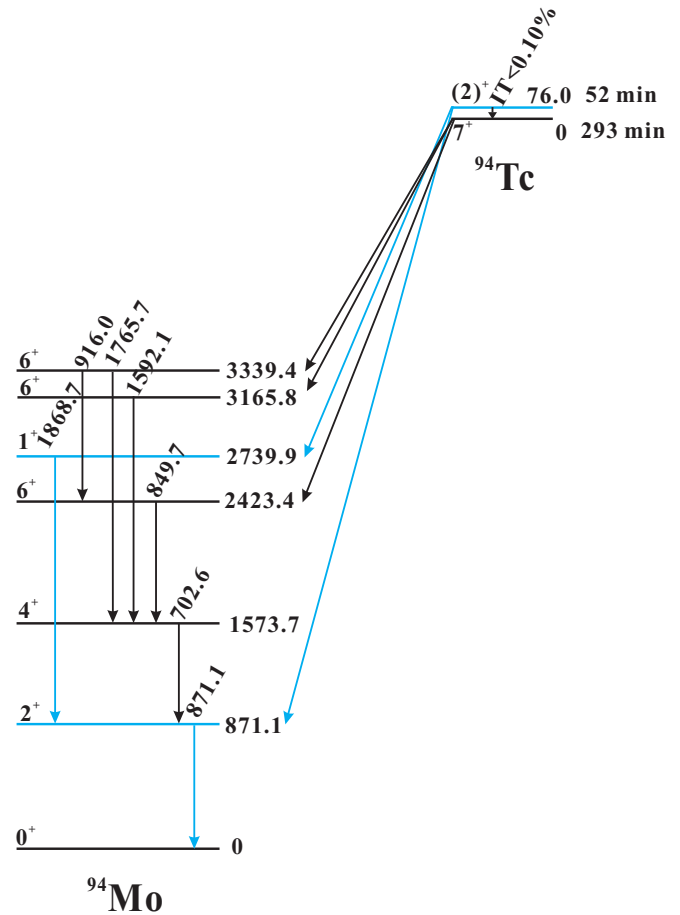


FIG. 1. Decay scheme of ^{94}Tc . The data are taken from Ref. [26], and only partial transitions are shown in the scheme.

$5n$ fusion evaporation channels. Of all these, $4n$ channel is the dominant one and takes about 70% of the total cross sections. Figure 1 shows the decay scheme of the ^{94}Tc , taken from Ref. [26]. It can be seen from the decay pattern that the nucleus can decay to ^{94}Mo through both $(2)^+$ isomeric state and the 7^+ ground state with different half-lives and characteristic γ rays. Therefore, these states can be identified unambiguously. Figure 2(a) presents the measured coincidence spectrum gated by the 1868.7-keV transition. The identification of the 871.1-keV transition in the figure clearly proves the decay sequence from the $(2)^+$ isomeric state. Figure 2(b) shows the 871.1-keV gated spectrum where 702.6-, 849.7-, and 916.0-keV transitions emerge, indicating identification of decay sequence from the 7^+ state. The energy range of the 871.1-keV-gated spectrum was extended to 2000-keV in Fig. 2(c) to show the weak lines. Other than this, it can also be noted that the 1868.7-keV γ ray could not be identified in the 871.1-keV-gated spectrum, confirming the dominance of decay sequence from the 7^+ state. To further justify the identification of the two states in ^{94}Tc , the half-lives of these states, i.e., the 7^+ (916.0-keV line) and $(2)^+$ (1868.7-keV line) are studied via radioactive decay curves as shown in Figs. 3(a) and 3(b), respectively. The lifetimes extracted in the present

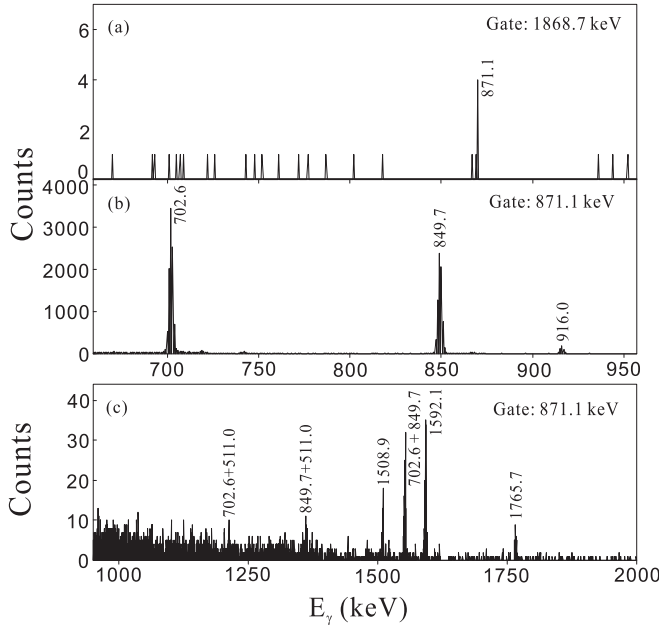


FIG. 2. Offline coincidence spectra measured from the decay of ^{94}Tc nucleus, gated by the (a) 1868.7-keV and (b) and (c) 871.1-keV transitions.

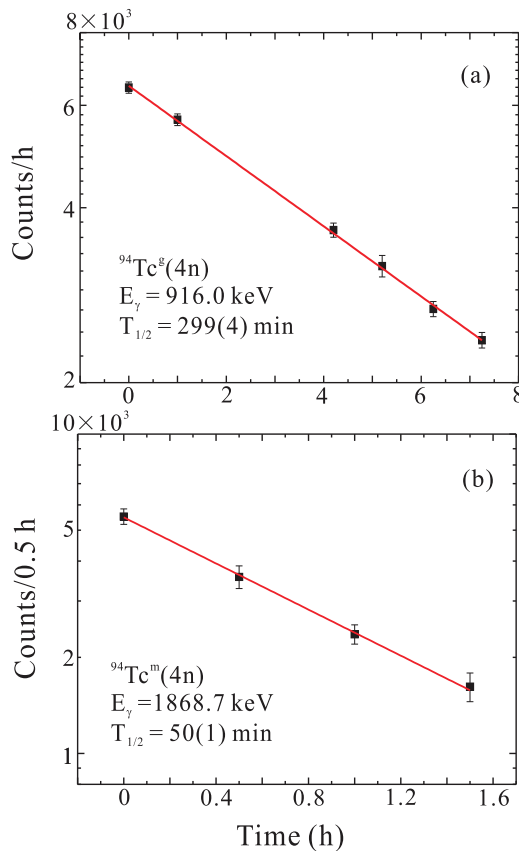


FIG. 3. Radioactive decay curves for the (a) $^{94}\text{Tc}^g$ and (b) $^{94}\text{Tc}^m$ states formed through the $^9\text{Be} + ^{89}\text{Y}$ reaction by using the 916.0- and 1868.7-keV transitions, respectively. See the text for details.

measurement are consistent with the values reported in the literature [26].

The experimental cross sections of the ^{94}Tc nucleus in the $^9\text{Be} + ^{89}\text{Y}$ reactions were extracted using the half-lives, prominent γ -ray energies of decay, and intensities following the method described in Refs. [23,27]. Note that the decay of isomeric state by isomeric transition (IT) is less than 0.1% [26], and it affects little on the estimation of the yield of the ground state. Fisichella *et al.* [28] have pointed out the possibility of inaccuracy of a derived excitation function observed mainly in the exponential region of cross section below the Coulomb barrier due to the ambiguities of derived beam energies. In this experiment, the beam energies are well above the barrier, and the changes in reaction cross sections are not dramatic. Therefore, the physics discussion for the present paper will not be affected much from the inaccuracy of the adopted beam energies. The extracted cross sections have been tabulated in Table I. The estimation of uncertainties have been performed by considering an $\approx 3\%$ error contribution each due to beam intensity, target thickness, and detector efficiency. The systematic uncertainties are added in quadrature to the statistical errors to get the total errors for the present measured cross sections. In practice, we found that the statistical errors make large contributions to the total errors due to the small branching ratio of decay from the isomeric state.

IV. COMPARISON WITH THEORETICAL CALCULATIONS

In order to further study the measured isomer yield ratios, we first tried to reproduce the total CF cross sections. As the ^9Be is weakly bound, it may break up before fusing with the target. In this case, there will be a possibility that the CF residues resulted from the capture of two ^4He particles following the breakup of ^9Be . This part of the residues is calculated using the PLATYPUS model [22]. A detailed description of the model has been presented in Refs. [29–31]. The other source of the residues considered in the calculation is the direct capture of ^9Be without breakup. The associated capture probabilities are obtained from a potential model calculation by solving the Schrödinger equation with the incoming-wave-boundary condition instead of using a sharp cutoff approximation as employed in the original PLATYPUS model (see, e.g., Eq. (4) in Ref. [30]). In all the calculations, the nuclear interaction potential was determined from the global Broglia-Winther parametrization [32]. The contribution from CF following breakup to the total CF was taken as 34%, extracted from the function in Ref. [33]. That function was resulted from the systematically fitting of the measured prompt-breakup probabilities. The comparison showing the calculated CF excitation functions as a function of $E_{c.m.}/V_B$ has been visualized in Fig. 4 with the experimental data taken from Ref. [23]. Here, $E_{c.m.}$ refers to the beam energy, and V_B is the Coulomb barrier energy, both in the center-of-mass frame. One can see from the red line in Fig. 4 that the predicted function is in agreement with the experimental data. We also compared the result assuming no breakup before fusion, determined solely by the potential model calculation as indicated by the blue line in the figure. Overall, this calculation has

TABLE I. Measured cross sections of isomeric state σ_m , ground-state σ_g , and the isomer ratios σ_m/σ_g for the ^{94}Tc formed in the $^9\text{Be} + ^{89}\text{Y}$ reaction system.

E_{lab} (MeV)	$E_{\text{c.m.}}/V_B$	$^{94}\text{Tc}^m$ (mb)	$^{94}\text{Tc}^g$ (mb)	$\sigma_m/\sigma_g(^{94}\text{Tc})$
50.1	2.14	18(3)	463(35)	0.039(8)
49.1	2.09	16(3)	460(33)	0.036(6)
48.1	2.05	22(2)	419(26)	0.053(7)
47.0	2.01	24(2)	412(24)	0.059(5)
45.9	1.96	23(3)	427(27)	0.053(7)

overestimated the experimental data, suggesting that the CF following breakup has to be considered in the analysis. Note that we have studied the CF cross sections combining the literature data of above barriers [14,16], and the necessity of including the ^9Be breakups in the full available energy range has been addressed in our previous work [23].

In the fusion evaporation reaction induced by heavy ions, the residues decay more favorably along the yrast lines, therefore, the transferred orbital angular momentum in the reaction is supposed to be the main factor affecting the isomer yield ratios. Since in the measured energy region the ^{94}Tc nucleus takes around 70% of total CF residues and the CF compound nucleus was chosen for study as it could be easily accessed. We have calculated the total spin distribution of the primary compound nucleus by adding the two sources of CF cross sections mentioned above, namely, the capture of two ^4He particles following the breakup of ^9Be and direct capture of ^9Be without breakup. The calculated results for the beam energies of 45.9 and 48.1 MeV are shown in Fig. 5 as examples. To get access to the isomer yield ratios, the phenomenological approach used in Refs. [34,35] was employed again to analyze the results. The obtained compound nucleus angular

momentum distribution was divided into two regions for calculating the relative population of the isomeric state to the ground state with a cutoff angular momentum J_{eff} . The region with low angular momentum feeds the $(2)^+$ state, and the region with high angular momentum feeds the 7^+ state. To account for the spread in the angular momentum possibly due to the neutron evaporation, a spreading parameter δ was introduced [34]. The isomer yield ratios were calculated as follows:

$$R = \frac{\sum_J \sigma_J^{(2)}}{\sum_J \sigma_J^{(1)}}, \quad (1)$$

$$\sigma_J^{(1)} = \frac{\sigma_J}{1 + \exp\left(\frac{J_{\text{eff}} - J}{\delta}\right)}, \quad (2)$$

$$\sigma_J^{(2)} = \frac{\sigma_J}{1 + \exp\left(\frac{J - J_{\text{eff}}}{\delta}\right)}, \quad (3)$$

where σ_J represents the cross section as a function of the total angular momentum distribution, and $\sigma_J^{(1)}$ and $\sigma_J^{(2)}$ refer to the cross sections associated with the ground state and isomeric state, respectively [34]. As an example, Fig. 5 also shows the division of population between the ground and the isomeric states of CF products at a beam energy of 45.9 MeV with $J_{\text{eff}} = 4\hbar$ and $\delta = 0.5$.

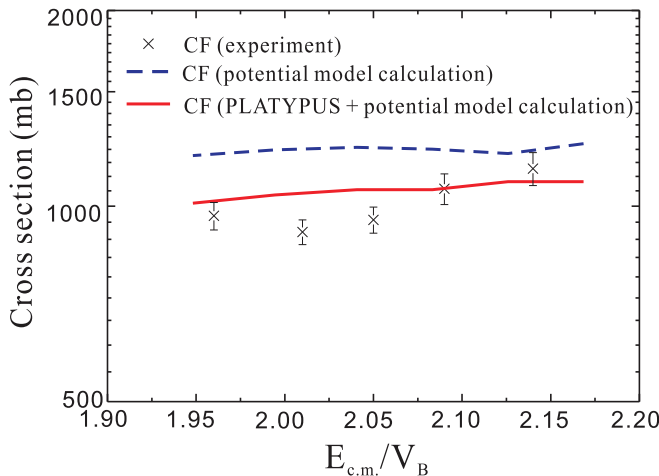


FIG. 4. Measured and calculated excitation functions for the complete fusion of the $^9\text{Be} + ^{89}\text{Y}$ system at above barrier energies. The blue dashed line refers to the result from the potential model calculation, assuming direct CF of the projectile-target without breakup. The red line corresponds to the result from the PLATYPUS model combined with the potential model calculation, assuming partial contribution (34%) from CF following breakup. The experimental data have been presented in Ref. [23]. See the text for details.

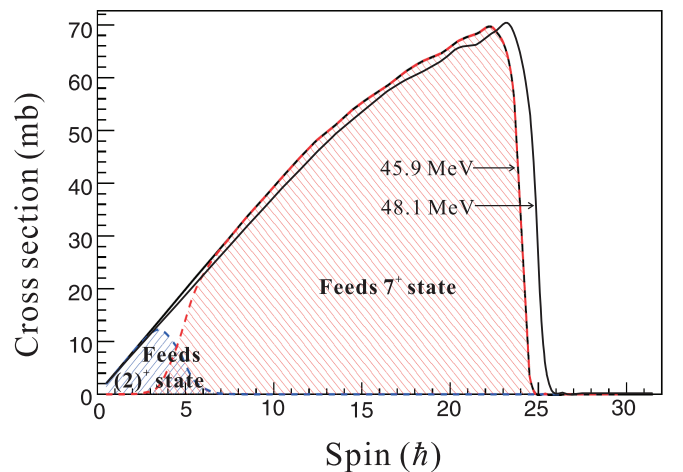


FIG. 5. Calculated angular momentum distribution for compound nucleus from CF of the $^9\text{Be} + ^{89}\text{Y}$ system at beam energies of 45.9 and 48.1 MeV. The division of population between the ground and the isomeric states at 45.9 MeV is indicated by the blue and red lines with $J_{\text{eff}} = 4\hbar$ and $\delta = 0.5$. See the text for details.

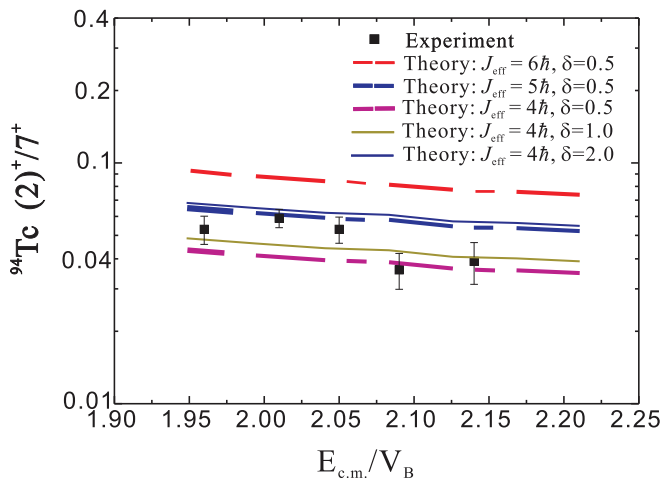


FIG. 6. The calculated and measured isomer ratios for ^{94}Tc formed through the $^9\text{Be} + ^{89}\text{Y}$ system, assuming different J_{eff} 's and δ values. See the text for details.

As a starting point, to check the dependence of extracted isomer ratio on the cutoff angular momentum J_{eff} , we fixed the spreading parameter δ as 0.5 and calculated the ratios for ^{94}Tc with $J_{\text{eff}} = 6, 5$, and $4\hbar$. The results are shown by thick lines in Fig. 6, together with the corresponding experimental data. On comparison, it was observed that the result obtained with $J_{\text{eff}} = 4\hbar$ is more close to the experimental data. To further explore the dependence of our approach on the spreading parameter, δ values are varied with 1.0 and 2.0, keeping the J_{eff} fixed. It revealed that a higher δ gives a higher isomer yield ratio. The almost close behaviors of predicted values are observed for the $J_{\text{eff}} = 4$ and $\delta = 2.0$ and $J_{\text{eff}} = 5$ and $\delta = 0.5$. This indicates that in this phenomenological approach neither the fixed cutoff angular momentum nor the fixed spreading parameter is appropriate to describe the data, and only a combination of the two is sufficient. Note that if we fixed the $J_{\text{eff}} = 7\hbar$, which is equal to the spin of ground state, no matter what value is chosen for δ , the predicted isomer yield ratios are always larger than the experimental data. This suggests that the predicted angular momentum for ^{94}Tc is overall insufficient to reproduce the experimental data. Otherwise, if the predicted angular momentum was higher, there would be more 7^+ states supposed to be populated, and in this way the deduced ratio of $(2)^+/7^+$ will be lower.

To further test our theoretical approach, the isomer yield ratios in ^{94}Tc from $^{93}\text{Nb}(^3\text{He}, 2n)$ reactions were studied additionally. For this paper we chose the energies from Coulomb barrier to $1.2E_{\text{c.m.}}/V_B$ as in this region the ^{94}Tc is predominant upon all CF residues, thus, the easily accessed CF compound nucleus could be selected for study. Figure 7(a) presents the comparison of experimental CF cross sections with theoretical predictions. The experimental values were deduced from the total ^{94}Tc cross sections [36] by considering their percentages in CF values from the PACE [37] predictions. The theoretical curve was obtained with the potential model calculation, which was adopted to calculate the $^9\text{Be} + ^{89}\text{Y}$ reaction system as shown in Fig. 4. Note that the breakup of the projectile was not considered in this calculation. The agreement between the theoretical curve and the experimental data in Fig. 7(a) is

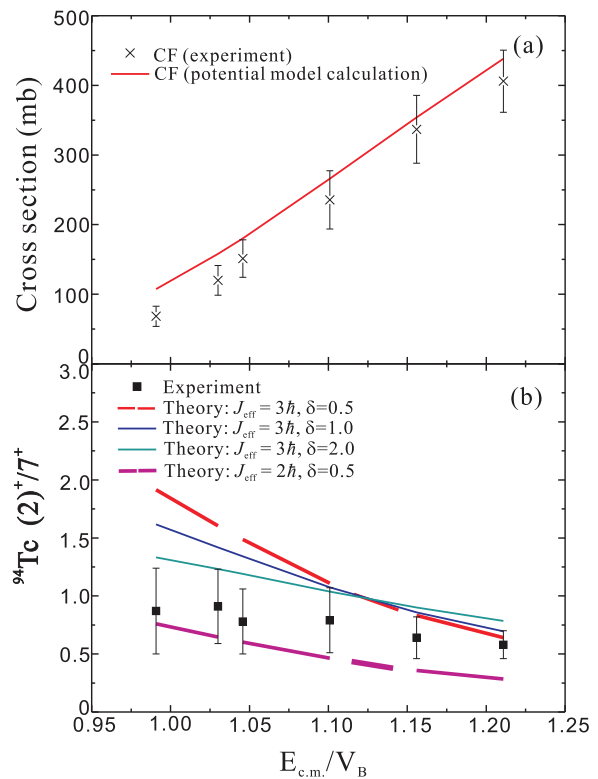


FIG. 7. (a) The measured and calculated complete fusion cross sections of the $^3\text{He} + ^{93}\text{Nb}$ system at above barrier energies. The experimental data are deduced using cross sections from Ref. [36]. The theoretical curve results from the potential model calculation. (b) The measured [36] and calculated isomer yield ratios for the ^{94}Tc using different J_{eff} 's and δ values. See the text for details.

good, considering that a global nuclear interaction potential has been used in the fusion calculations. Using a similar approach as that for the $^9\text{Be} + ^{89}\text{Y}$ system, the deduced isomer yield ratios of ^{94}Tc formed through the $^3\text{He} + ^{93}\text{Nb}$ system are shown in Fig. 7(b). One can see from the figure that the results obtained from $J_{\text{eff}} = 3\hbar$ and $J_{\text{eff}} = 2\hbar$ are close to the experimental data. Adopting a $J_{\text{eff}} = 7\hbar$ will give much higher predictions compared to the experimental value. This gives the indication again that the predicted angular momentum for ^{94}Tc is not enough.

After the compound nucleus was formed in the reaction, the angular momentum of ^{94}Tc would be affected by the emitted neutrons. This may be one of the reasons that the predictions with $J_{\text{eff}} = 7\hbar$ are higher than the measured isomer yield ratios. Other than the factors discussed above there also exist some factors which have impacts on the isomer yield ratios in the experiment. For example, the distribution of excitation energy in the compound nucleus may lead to tentatiousness to certain states, the γ quantum emitted during the deexcitation may shift the angular momentum distribution of the compound nucleus. In these cases, unlike the above adopted phenomenological approach, only the spreading of the angular momentum at a cutoff spin may not be enough. Therefore, the complete knowledge of the decay path of the compound nuclei is required to accurately describe the isomer ratio data.

V. SUMMARY

For the present paper, the ${}^9\text{Be} + {}^{89}\text{Y}$ reaction has been used to populate the ${}^{94}\text{Tc}$ nucleus. The isomer yield ratios have been measured through a standard stacked-foil irradiation by the ${}^9\text{Be}$ beam followed by an offline measurement of the γ rays from reaction residues. In the theoretical analysis, the role of CF following breakup was considered by employing the PLATYPUS model, and the role of direct CF without breakup was determined by the potential model calculation. The combination of two roles gives an adequate description of experimental excitation functions, even the precise distinction between the two processes could not be established experimentally. In contrast, the direct potential model calculation without considering CF following breakup overestimated the experimental data. By employing a phenomenological approach, the angular momentum distribution has been studied with a cutoff spin and a spreading parameter. The approach managed to reproduce the experimental isomer ratio data qualitatively and on the order of magnitude. We also tested the approach using the isomer yield ratios from the ${}^3\text{He} + {}^{93}\text{Nb}$ system and obtained a similar result. Overall, the predicted

angular momentum is insufficient to accurately reproduce the experimental data. More precise knowledge is still needed to completely describe the decay path of the compound nucleus, the spread of angular momentum, and ultimately the measured isomer yield ratios. The analysis of the ${}^9\text{Be} + {}^{89}\text{Y}$ and ${}^3\text{He} + {}^{93}\text{Nb}$ systems offers the opportunity to further compare other projectile-target combinations and deeply understand the reaction mechanisms. This paper also extends information on the production of the ${}^{94}\text{Tc}$ nucleus—one of the promising candidates in the application of medical diagnostics.

ACKNOWLEDGMENTS

The work at the Institute of Modern Physics, CAS was supported by the Youth Innovation Promotion Association of Chinese Academy of Sciences (Grant No. 2019407), the Strategic Priority Research Program of Chinese Academy of Sciences (Grant No. XDB34010000), and the National Natural Science Foundation of China (Grants No. U1932138, No. U1832134, No. 11775274, and No. 11305221). The work at the University of Surrey was supported by the STFC (Grant No. ST/P005314/1).

-
- [1] T. J. Ruth, *Rep. Prog. Phys.* **72**, 016701 (2008).
 [2] T. Hayakawa, Y. Hatsukawa, and T. Tanimori, *Heliyon* **4**, e00497 (2018).
 [3] C. Hoehr, T. Morley, K. Buckley, M. Trinczek, V. Hanemaayer, P. Schaffer, T. Ruth, and F. Bénard, *Appl. Radiat. Isot.* **70**, 2308 (2012).
 [4] K. Gagnon, S. McQuarrie, D. Abrams, A. J. McEwan, and F. Wuest, *Curr. Radiopharm.* **4**, 90 (2011).
 [5] B. T. Christian, R. J. Nickles, C. K. Stone, T. L. Mulnix, and J. Clark, *Appl. Radiat. Isot.* **46**, 69 (1995).
 [6] J. J. Hogan, *J. Inorg. Nucl. Chem.* **35**, 705 (1973).
 [7] G. Galy, B. Philippon, A. Bardy, and R. Munsch, *Int. J. Appl. Radiat. Isot.* **32**, 277 (1981).
 [8] M. Izumo, H. Matsuoka, T. Sorita, Y. Nagame, T. Sekine, K. Hata, and S. Baba, *Int. J. Radiat. Appl. Instrum. Part A. Appl. Radiat. Isot.* **42**, 297 (1991).
 [9] F. Tárkányi, F. Ditrói, A. Hermanne, S. Takács, and A. Ignatyuk, *Nucl. Instrum. Methods Phys. Res., Sect. B* **280**, 45 (2012).
 [10] B. Strohmaier, M. Faßbender, and S. M. Qaim, *Phys. Rev. C* **56**, 2654 (1997).
 [11] J. Zaidi, M. Arif, S. Ahmed, and I. Qureshi, *Radiochim. Acta* **85**, 9 (1999).
 [12] J. Zaidi, M. Arif, I. Fatima, S. Waheed, S. Ahmad, and I. Qureshi, *Radiochim. Acta* **93**, 547 (2005).
 [13] K. Gagnon, F. Bénard, M. Kovacs, T. J. Ruth, P. Schaffer, J. S. Wilson, and S. A. McQuarrie, *Nucl. Med. Biol.* **38**, 907 (2011).
 [14] M. Maiti and S. Lahiri, *Phys. Rev. C* **81**, 024603 (2010).
 [15] B. B. Kumar, S. Mukherjee, S. Chakrabarty, B. S. Tomar, A. Goswami, and S. B. Manohar, *Phys. Rev. C* **57**, 743 (1998).
 [16] C. S. Palshetkar, S. Santra, A. Chatterjee, K. Ramachandran, S. Thakur, S. K. Pandit, K. Mahata, A. Shrivastava, V. V. Parkar, and V. Nanal, *Phys. Rev. C* **82**, 044608 (2010).
 [17] A. Diaz-Torres and I. J. Thompson, *Phys. Rev. C* **65**, 024606 (2002).
 [18] A. Diaz-Torres, I. J. Thompson, and C. Beck, *Phys. Rev. C* **68**, 044607 (2003).
 [19] I. J. Thompson and A. Diaz-Torres, *Prog. Theor. Phys. Suppl.* **154**, 69 (2004).
 [20] K. Yabana, *Prog. Theor. Phys.* **97**, 437 (1997).
 [21] M. Boselli and A. Diaz-Torres, *Phys. Rev. C* **92**, 044610 (2015).
 [22] A. Diaz-Torres, *Comput. Phys. Commun.* **182**, 1100 (2011).
 [23] G. S. Li, M. L. Liu, D. Patel, Y. D. Fang, X. H. Zhou, Y. H. Zhang, A. Diaz-Torres, C. S. Palshetkar, J. Lubian, N. T. Zhang *et al.*, *Phys. Rev. C* **101**, 014606 (2020).
 [24] D. Bazin, O. Tarasov, M. Lewitowicz, and O. Sorlin, *Nucl. Instrum. Methods Phys. Res., Sect. A* **482**, 307 (2002).
 [25] C. Scheidenberger and H. Geissel, *Nucl. Instrum. Methods Phys. Res., Sect. B* **135**, 25 (1998).
 [26] D. Abriola and A. Sonzogni, *Nucl. Data Sheets* **107**, 2423 (2006).
 [27] N. T. Zhang, Y. D. Fang, P. R. S. Gomes, J. Lubian, M. L. Liu, X. H. Zhou, G. S. Li, J. G. Wang, S. Guo, Y. H. Qiang *et al.*, *Phys. Rev. C* **90**, 024621 (2014).
 [28] M. Fisichella, A. C. Shotter, A. Di Pietro, P. Figuera, M. Lattuada, C. Marchetta, V. Privitera, L. Romano, C. Ruiz, and M. Zadro, *Phys. Rev. C* **92**, 064611 (2015).
 [29] A. Diaz-Torres, D. J. Hinde, J. A. Tostevin, M. Dasgupta, and L. R. Gasques, *Phys. Rev. Lett.* **98**, 152701 (2007).
 [30] A. Diaz-Torres, *J. Phys. G: Nucl. Part. Phys.* **37**, 075109 (2010).
 [31] A. Diaz-Torres and D. Quraishi, *Phys. Rev. C* **97**, 024611 (2018).
 [32] W. Reisdorf, *J. Phys. G: Nucl. Part. Phys.* **20**, 1297 (1994).
 [33] B. Wang, W.-J. Zhao, A. Diaz-Torres, E.-G. Zhao, and S.-G. Zhou, *Phys. Rev. C* **93**, 014615 (2016).
 [34] L. R. Gasques, M. Dasgupta, D. J. Hinde, T. Peatey, A. Diaz-Torres, and J. O. Newton, *Phys. Rev. C* **74**, 064615 (2006).
 [35] G. S. Li, Y. D. Fang, A. Diaz-Torres, M. L. Liu, N. T. Zhang, X. H. Zhou, Y. H. Zhang, J. G. Wang, B. S. Gao, Y. H. Qiang *et al.*, *Phys. Rev. C* **99**, 054617 (2019).
 [36] M. Faßbender, A. F. Novgorodov, F. Rösch, and S. M. Qaim, *Radiochim. Acta* **65**, 215 (1994).
 [37] A. Gavron, *Phys. Rev. C* **21**, 230 (1980).